Mechanistic Insights into the Reaction between VO_2^+ and Propene Based on a DFT Study

L. Gracia,† J. R. Sambrano,‡ J. Andrés,*,† and A. Beltrán†

Departament de Ciències Experimentals, Universitat Jaume I, Box 224, 12080 Castelló, Spain, and Laboratorio de Simulaçào Molecular, DM, Unesp, Universidade Estadual Paulista, Box 473, 17033-360 Bauru, Brazil

Received November 11, 2005

Calculations based on density functional theory have been carried out to investigate the free energy profiles at singlet and triplet electronic states associated with the gas-phase ion/molecule reactions of VO_2^+ ($^1A_1/^3A''$) with propene. The complex potential energy surfaces, including six reaction pathways (three dehydrogenation and three oxygen transfer processes), have been explored and analyzed. Along dehydrogenation reactive channels, three final products can be obtained: $V(OH)_2^+$ ($^1\Sigma^+/^3\Sigma^-$) and allene (*path Deh1*), being the most kinetically and thermodynamically favorable reaction pathway, $V(OH)_2^+$ ($^1\Sigma^+/^3\Sigma^-$) and propyne (*path Deh2*), and VO_2^+ ($^1A_1/^3A''$) and H_2 plus allene (*path Deh3*). The oxygenation processes can yield as final products VO^+ ($^1\Delta/^3\Sigma$) and acetone (*path Ox1*), VO^+ ($^1\Delta/^3\Sigma$) and propanaldehyde (*path Ox2*), and VO^+ ($^1\Delta/^3\Sigma$) and H_2 and propenaldehyde (*path Ox3*). Both *paths Deh1* and *Deh2* are associated with two consecutive hydrogen transfer processes from carbon atoms of the propene fragment to vanadyl oxygen atoms, while in *path Deh3* the second hydrogen migration takes place to the vanadium atom followed by the formation of a hydrogen molecule. Both *paths Ox1* and *Ox2* comprise an intramolecular hydrogen transfer between the ethylenic moiety of the propene fragment, while two consecutive hydrogen transfer processes take place from the propene fragment to oxygen and vanadium atoms of the vanadyl moiety along *path Ox3*. Three crossing points between both electronic states take place along *path Deh1* (**CP-*Deh1***) and *path Deh2* (**CP-*Deh2***) and in the entrance channel of oxidation processes (**CP-*Ox***). A comparison with previous works on related reactions $VO_2^+ + C_2H_4$, $VO_2^+ + C_2H_6$, and $VO_2^+ + C_3H_8$ allows us to rationalize the different reactivity patterns.

1. Introduction

The key role of transition metal oxides in a wide range of technological applications[1] justifies that their gas-phase reactions are the subject of numerous studies,[2−12] and in particular, the oxidation of hydrocarbons is involved in the major portion of catalytic processes.[13−15] Selective oxidation of lower unsaturated or saturated hydrocarbons is of fundamental and technological interest because it provides a potential route to effectively transform lower hydrocarbons to higher, value-added chemicals.[16−19]

The interaction between organic molecules and small metal clusters has attained the attention of theoreticians and experimentalists not only because they can be used as models for more complex catalytic processes but also for the intrinsic importance of this subject. In that respect, some fundamental insight might be gained by studying the reactivity at metal centers and to extrapolate some information on the interactions that occur on metal oxide surfaces. Vanadium oxides have commanded considerable attention because of their numerous potential industrial and catalytic applications.[20−26] Therefore, several

* To whom correspondence should be addressed. Phone: +34 964 728072. Fax: +34 964728066. E-mail: andres@exp.uji.es.

† Universitat Jaume I.

‡ Universidade Estadual Paulista.

(1) Henrich, V. E.; Cox, P. A. *The Surface Science of Metal Oxides*; Cambridge University Press: New York, 1994.

(2) Fiedler, A.; Schroder, D.; Shaik, S.; Schwarz, H. *J. Am. Chem. Soc.* **1994**, *116*, 10734−10741.

(3) Fiedler, A.; Kretzschmar, I.; Schroder, D.; Schwarz, H. *J. Am. Chem. Soc.* **1996**, *118*, 9941−9952.

(4) Harvey, J. N.; Aschi, M. *Phys. Chem. Chem. Phys.* **1999**, *1*, 5555−5563.

(5) Schröder, D.; Shaik, S.; Schwarz, H. *Acc. Chem. Res.* **2000**, *33*, 139−145.

(6) Ogliaro, F.; Harris, N.; Cohen, S.; Filatov, M.; de Visser, S. P.; Shaik, S. *J. Am. Chem. Soc.* **2000**, *122*, 8977−8989.

(7) Zemski, K. A.; Bell, R. C.; Castleman, A. W. *J. Phys. Chem. A* **2000**, *104*, 5732−5741.

(8) Zemski, K. A.; Justes, D. R.; Castleman, A. W. *J. Phys. Chem. A* **2001**, *105*, 10237−10245.

(9) Oyama, S. T.; Radhakrishnan, R.; Seman, M.; Kondo, J. N.; Domen, K.; Asakura, K. *J. Phys. Chem. B* **2003**, *107*, 1845−1852.

(10) Fielicke, A.; Meijer, G.; von Helden, G. *Eur. Phys. J. D* **2003**, *24*, 69−72.

(11) Justes, D. R.; Moore, N. A.; W., C. A. *J. Phys. Chem. B* **2004**, *108*, 3855−3862.

(12) Engeser, M.; Schroder, D.; Schwarz, H. *Chem. Eur. J.* **2005**, *11*, 5975−5987.

(13) Oyama, S. T.; Hightower, J. W. *Catalytic Selective Oxidation*; American Chemical Society: Washington, DC, 1993.

(14) Warren, B. K.; Oyama, S. T. *Heterogeneous Hydrocarbon Oxidation*; American Chemical Society: Washington, DC, 1996.

(15) Hodnett, B. K. *Heterogeneous Catalytic Oxidation*; John Wiley & Sons Ltd.: New York, 2000.

(16) Weissermel, K.; Arpe, H.-J. *Organic Synthesis by Oxidation with Metal Compounds*; Plenum: New York, 1986.

(17) Bettahar, M. M.; Costentin, G.; Savary, L.; Lavalley, J. C. *Appl. Catal. A* **1996**, *145*, 1−48.

(18) Weissermel, K.; Arpe, H.-J. *Industrial Organic Chemistry*; VCH: Weinheim, 1997.

(19) Olah, G. A.; Molnar, A. *Hydrocarbon Chemistry*; John Wiley & Sons: Hoboken, NJ, 2003.

(20) Kung, H. H. *Transition Metal Oxides: Surface Chemistry and Catalysis, Studies in Surface Science and Catalysis*; Elsevier: Amsterdam, 1989.

(21) Escribano, V. S.; Busca, G.; Lorenzelli, V. *J. Phys. Chem.* **1990**, *94*, 8945−8950.

(22) Oyama, S. T.; Somorjai, G. A. *J. Phys. Chem.* **1990**, *94*, 5022−5028.

(23) Topsoe, N.-Y. *Science* **1994**, *265*, 1217−1219.

10.1021/om050971t CCC: $33.50
Publication on Web 03/02/2006

experimental[27−39] and theoretical[39−47] studies on the structure of ionic vanadium oxide clusters of different stoichiometries, $V_xO_y^{+/-}$, have been presented and their interactions with various compounds such as hydrocarbons, alkyl halides, or methanol[11,12,37,48−50] have been studied in order to provide valuable information on the structure−reactivity relationships and to offer a new insight into the nature of active sites responsible for the reaction under investigation.

Many chemical processes involve transitions between multielectronic states of different spin multiplicity. Such transitions, not being electric dipole allowed, are formally spin forbidden and are often interpreted in terms of the crossing of two energy surfaces. Chemical reactivity associated with metal oxide cations is a well-recognized example of two-state reactivity,[5,51,52] reported by Schröder, Schwarz, and Shaik, and it is a new concept for describing the course of a chemical reaction in the context of interspin crossing. In this case, the changes between two or more different electronic states are known to accompany the progress of the reaction and can modify the efficiency and/or selectivity of a given chemical rearrangement and can also influence a reaction from a process without change in spin state to a situation where the spin change completely determines the rate and selectivity. There are still a lot of mechanistic details of the activation process to be solved; thus, understanding the mechanism of this type of chemical reaction is of great interest from both a practical and a fundamental point of view, as recently illustrated by Poli and Harvey with the spin-forbidden reactions in organometallic complexes,[31,53,54] but also in different fields such as atmospheric chemistry,[55] astrochemistry,[56] many inorganic,[57] organic,[58−60] and biochemical reactions,[61] reactions with participation of dirradicals,[62] and metal surface reactions.[63] Even, recently Shaik et al.[64] pointed out the presence of four electronic states to understand the mechanism of hydroxylation and epoxidation by cytochrome P450. Schwarz[52] emphasizes that multistate reactivity patterns are much more important than generally acknowledged, and he reviews examples where a fruitful intersection of experimental and computational studies is reached, while Mercero et al. have recently stressed the widely used methods in quantum chemistry that illustrate the applica-

(24) Rao, C. N.; Raven, B. *Transition Metal Oxides*; VCH: New York, 1995.

(25) Haggin, J. *Chem. Eng. News* **1995**, *73*, 20−23.

(26) Ruth, K.; Burch, R.; Kieffer, R. *J. Catal.* **1998**, *175*, 27−39.

(27) Bell, R. C.; Zemski, K. A.; Kerns, K. P.; Deng, H. T.; Castleman, A. W. *J. Phys. Chem. A* **1998**, *102*, 1733−1742.

(28) Bell, R. C.; Zemski, K. A.; Castleman, A. W. *J. Cluster Sci.* **1999**, *10*, 509−524.

(29) Bell, R. C.; Zemski, K. A.; Castleman Jr, A. W. *J. Phys. Chem. A* **1999**, *103*, 2992−2998.

(30) Foltin, M.; Stueber, G. J.; Bernstein, E. R. *J. Chem. Phys.* **1999**, *111*, 9577−9586.

(31) Harvey, J. N.; Diefenbach, J. N.; Schröder, D.; Schwarz, H. *Int. J. Mass Spectrom.* **1999**, *182/183*, 85−97.

(32) Bell, R. C.; Zemski, K. A.; Justes, D. R.; Castleman, A. W. *J. Chem. Phys.* **2001**, *114*, 798−811.

(33) Fielicke, A.; Rademann, K. *Phys. Chem. Chem. Phys.* **2002**, *4*, 2621−2628.

(34) Zemski, K. A.; Justes, D. R.; Castleman, A. W. *J. Phys. Chem. B* **2002**, *106*, 6136−6148.

(35) Asmis, K. R.; Brummer, M.; Kaposta, C.; Santambrogio, G.; von Helden, G.; Meijer, G.; Rademann, K.; Woste, L. *Phys. Chem. Chem. Phys.* **2002**, *4*, 1101−1104.

(36) Schroder, D.; Engeser, M.; Bronstrup, M.; Daniel, C.; Spandl, J.; Hartl, H. *Int. J. Mass Spectrom.* **2003**, *228*, 743−757.

(37) Engeser, M.; Schlangen, M.; Schroder, D.; Schwarz, H.; Yumura, T.; Yoshizawa, K. *Organometallics* **2003**, *22*, 3933−3943.

(38) Schroder, D.; Loos, J.; Engeser, M.; Schwarz, H.; Jankowiak, H. C.; Berger, R.; Thissen, R.; Dutuit, O.; Dobler, J.; Sauer, J. *Inorg. Chem.* **2004**, *43*, 1976−1985.

(39) Asmis, K. R.; Meijer, G.; Brümmer, M.; Kaposta, C.; Santambrogio, G.; L., W.; Sauer, J. *J. Chem. Phys.* **2004**, *120*, 6461−6470.

(40) Vyboishchikov, S. F.; Sauer, J. *J. Phys. Chem. A* **2000**, *104*, 10913−10922.

(41) Vyboishchikov, S. F.; Sauer, J. *J. Phys. Chem. A* **2001**, *105*, 8588−8598.

(42) Calatayud, M.; Andrés, J.; Beltrán, A.; Silvi, B. *Theor. Chem. Acc.* **2001**, *105*, 299−308.

(43) Calatayud, M.; Silvi, B.; Andrés, J.; Beltrán, A. *Chem. Phys. Lett.* **2001**, *333*, 493−503.

(44) Calatayud, M.; Andrés, J.; Beltrán, A. *J. Phys. Chem. A* **2001**, *105*, 9760−9775.

(45) Calatayud, M.; Berski, S.; Beltran, A.; Andres, J. *Theor. Chem. Acc.* **2002**, *108*, 12−20.

(46) Pykavy, M.; van Wullen, C. *J. Phys. Chem. A* **2003**, *107*, 5566−5572.

(47) Molec, K. S.; Jaeger, T. D.; Duncan, M. A. *J. Chem. Phys.* **2005**, *123*, in press.

(48) Justes, D. R.; Mitric, R.; Moore, N. A.; Bonacic-Koutecky, V.; Castleman, A. W., Jr. *J. Am. Chem. Soc.* **2003**, *125*, 6289−6299.

(49) Justes, D. R.; Castleman, A. W.; Mitric, R.; Bonacic-Koutecky, V. *Eur. Phys. J. D* **2003**, *24*, 331−334.

(50) Vyboishchikov, S. F. *J. Mol. Struct. Theochem.* **2005**, *723*, 53−61.

(51) Schröder, D.; Schwarz, H.; Shaik, S. *Metal-oxo and metal-peroxo species in catalytic oxidations*; Springer-Verlag: Berlin, 2000.

(52) Schwarz, H. *Int. J. Mass Spectrom.* **2004**, *237*, 75−105.

(53) Harvey, J. N.; Aschi, M.; Schwarz, H.; Koch, W. *Theor. Chem. Acc.* **1998**, *99*, 95−99.

(54) Oiestad, E. L.; Harvey, J. N.; Uggerud, E. *J. Phys. Chem. A* **2000**, *104*, 8382−8388. Smith, K. M.; Poli, R.; Harvey, J. N. *Chem. Eur. J.* **2001**, *7*, 1679−1690. Harvey, J. N.; Poli, R.; Smith, K. M. *Coord. Chem. Rev.* **2003**, *238−239*, 347−361. Poli, R.; Harvey, J. N. *Chem. Soc. Rev.* **2003**, *32*, 1−8. Poli, R. *J. Organomet. Chem.* **2004**, *689*, 4291−4304. Carreón-Macedo, J. L.; Harvey, J. N. *J. Am. Chem. Soc.* **2004**, *126*, 5789−5797. Carreón-Macedo, J.; Harvey, J. N.; Poli, R. *Eur. J. Inorg. Chem.* **2005**, 2999−3008.

(55) Yarkony, D. R. *J. Am. Chem. Soc.* **1992**, *114*, 5406−5411.

(56) Flores, J. R.; Barrientos, C.; Largo, A. *J. Phys. Chem.* **1994**, *98*, 1090−1099.

(57) Agren, H.; Vahtras, O.; Minaev, B. F. *Adv. Quantum Chem.* **1996**, *27*, 71. Kretzchmar, I.; Schröder, D.; Schwarz, H.; Rue, C.; Armentrout, P. B. *J. Phys. Chem. A* **1998**, *102*, 10060−10073. Yoshizawa, K.; Shiota, Y.; Yamabe, T. *Organometallics* **1998**, *17*, 2825−2831. Filatov, M.; Shaik, S. *J. Phys. Chem. A* **1998**, *102*, 3835−3846. Rue, C.; Armentrout, P. B.; Kretzchmar, I.; Schröder, D.; Harvey, J. N.; Schwarz, H. *J. Chem. Phys.* **1999**, *110*, 7858−7870. Minaev, B. F.; Agren, H. *EPA Newslett.* **1999**, *65*, 7. Yoshizawa, K.; Shiota, Y.; Yamabe, T. *J. Chem. Phys.* **1999**, *111*, 538−545. Yoshizawa, K.; Shiota, Y.; Yamabe, T. *J. Am. Chem. Soc.* **1999**, *121*, 147−153. Harris, N.; Shaik, S.; Schröder, D.; Schwarz, H. *Helv. Chim. Acta* **1999**, *82*, 1784−1797. Irigoras, A.; Fowler, J. E.; Ugalde, J. M. *J. Am. Chem. Soc.* **1999**, *121*, 8549−8558. Gorelsky, S. I.; Lavrov, V. V.; Koyanagi, G. K.; Hopkinson, A. C.; Bohme, D. K. *J. Phys. Chem. A* **2001**, *105*, 9410−9414. Chiodo, S.; Kondakova, O.; Michelini, M. D.; Russo, N.; Sicilia, E. *Inorg. Chem.* **2003**, *42*, 8773−8782. Chiodo, S.; Kondakova, O.; Michelini, M. D.; Russo, N.; Sicilia, E.; Irigoras, A.; Ugalde, J. M. *J. Phys. Chem. A* **2004**, *108*, 1069−1081. Zhang, G.; Li, S.; Jiang, Y. *Organometallics* **2004**, *23*, 3656−3667. Ishikawa, T.; Tanaka, K. *J. Chem. Phys.* **2005**, *122*, in press. Iwakura, I.; Ikeno, T.; Yamada, T. *Angew. Chem., Int. Ed.* **2005**, *44*, 2524−2527.

(58) Hess, B. A.; Marian, C. M.; Peyerimhoff, S. D. In *Modern Electronic Structure Theory*; Yarkoni, D. R., Ed.; World Scientific: Singapore, 1995.

(59) Klessinger, M.; Michl, J. *Excited States and Photochemistry of Organic Molecules*; New York, 1995.

(60) Musaev, D. G.; Morokuma, K. *J. Phys. Chem.* **1996**, *100*, 11600−11609. Fiedler, A.; Schröder, D.; Zummack, W.; Schwarz, H. *Inorg. Chim. Acta* **1997**, *259*, 227−235. Aschi, M.; Largo, A. *Chem. Phys.* **2001**, *265*, 251−261. Michelini, M. D.; Russo, N.; Sicilia, E. *J. Phys. Chem. A* **2002**, *106*, 8937−8944. Limberg, C. *Angew. Chem., Int. Ed.* **2003**, *42*, 5932−5954. Michelini, M. D.; Sicilia, E.; Russo, N.; Alikhani, M. E.; Silvi, B. *J. Phys. Chem. A* **2003**, *107*, 4862−4868. Michelini, M. D.; Russo, N.; Alikhani, M. E.; Silvi, B. *J. Comput. Chem. A* **2004**, *25*, 1647−1655. Michelini, M. D.; Russo, N.; Alikhani, M. E.; Silvi, B. *J. Comput. Chem. A* **2005**, *26*, 1284−1293.

(61) Abashkin, Y. G.; Burt, S. K.; Russo, N. *J. Phys. Chem. A* **1997**, *101*, 8085−8093. Green, J. C.; Jardine, C. N. *J. Chem. Soc., Dalton Trans.* **1998**, 1057−1061. Shaik, S.; de Visser, S. P.; Ogliaro, F.; Schwarz, H.; Schröder, D. *Curr. Opin. Chem. Biol.* **2002**, *6*, 556−567.

(62) Salem, L.; Rowland, C. *Angew. Chem., Int. Ed. Engl.* **1972**, *11*, 92.

(63) Landis, C. R.; Morales, C. M.; Stahl, S. S. *J. Am. Chem. Soc.* **2004**, *126*, 16302−16303. Behler, J.; Delley, B.; Lorenz, S.; Reuter, K.; Scheffler, M. *Phys. Rev. Lett.* **2005**, *94*, in press. Fan, X. L.; Zhang, Y. F.; Lau, W. M.; Liu, Z. F. *Phys. Rev. Lett.* **2005**, *94*, in press.

(64) Hirao, H. K. D.; Thiel, W.; Shaik, S. *J. Am. Chem. Soc.* **2005**, *127*, 13007−13018.

tions of the theory on the spin-forbiddeness of gas-phase ion−molecule reactions.[65]

To contribute to the understanding of reactions of vanadium oxide cluster cations with hydrocarbons, such as alkanes and alkenes, in two recent publications we have presented a first-principle theoretical description of the reaction between VO_2^+ ($^1A_1/^3A''$) and ethene[66] and ethane.[67] The motivation is to facilitate an understanding of the role of electronic structures on mechanistic details at a molecular level, to clarify the dominant product channels, and to support mechanistic proposals based on experimental results, as well as to analyze potential energy surface (PES) crossing scenarios. This kind of knowledge is essential for understanding the whole reaction mechanism and is useful for establishing an appropriate model for the oxidation and dehydrogenation processes. This stimulates ongoing mechanistic studies and has led to the important finding that these reactions are multichannel processes with different spin states, and the possible crossing of potential surfaces is emphasized. In these cases, the origin of two-state reactivity was traced to the fact that the reactant presents a singlet (s) spin multiplicity, VO_2^+ ($^1A_1$), while the product has a triplet (t) spin multiplicity as the ground state, VO^+ ($^3\Sigma$), and various spin reaction channels point out different mechanistic pictures.

In view of the potential importance and the rather limited experimental information, a careful theoretical study of the s and t PES is desirable. Here, we report the first detailed density functional theory (DFT) study on the mechanism of the gas-phase reactions of VO_2^+ ($^1A_1/^3A''$) with propene C_3H_6 (^1A), combining simple and double carbon−carbon bonds as presented in ethane and ethene systems, respectively. This reaction can be considered as a model system for oxidation and hydrogenation catalysis at a molecular level, and the varied physical chemistry of this ion/molecule gas-phase reaction is analyzed from a quantum mechanical perspective. Accurate theoretical computations can offer an alternative source of information, and an interplay between theory and experiment is very helpful in this area of research, as recently pointed out by Schwarz.[52] Calculations including geometry optimizations, vibrational analysis, Gibbs free energy for the stationary points on PESs, and crossing points (CPs) between singlet and triplet electronic states have been carried out. Our ultimate purpose is to highlight the interesting help that theoretical calculations can bring in future experiments.

The organization of this paper is as follows: computing methods and model systems are summarized in section 2. In section 3, the results are reported, analyzed, and discussed; an overview of the stationary points, the results of the free energy profiles with a natural population analysis, and the characterization of the CPs is given; finally, a comparison with previous works on related systems is provided. The main conclusions are given in section 4.

2. Theoretical Methods

The calculations were performed using the GAUSSIAN03 program package.[68] We applied the same computational method as in previous studies,[66,67] the unrestricted B3LYP level,[69−71] in combination with the standard all-electron 6-311G(2d,p)[72] basis set to describe the atoms. The reason that we adopted this level and basis set was that we applied it to calculate the complex molecular mechanisms associated with the reactions $VO_2^+ + C_2H_4$[66] and $VO_2^+ + C_2H_6$[67] and the tautomerization process of $MO(H_2O)^+$[73] as well as previous works with complex systems involving vanadium oxide sytems[42−44] and they yielded satisfactory results. Therefore, we are confident with the calculated data at this computing level for this type of reaction.

The computed stationary points have been characterized as minima or transition states (TSs) by diagonalizing the Hessian matrix and analyzing the vibrational normal modes, employing the Berny algorithm for the geometry optimizations;[74] that is, equilibrium species possess all real frequencies, whereas TSs possess only one imaginary frequency. The particular nature of TSs has been determined by analyzing the motion described by the eigenvector associated with the imaginary frequency, the transition vector (TV).[75] Furthermore, the intrinsic reaction coordinate (IRC) method[76,77] has been used to describe minimum energy paths from TSs to the corresponding minima along the imaginary mode of vibration using the algorithm developed by González and Schlegel[78] in the mass-weighted internal coordinate system. Thus, harmonic vibrational frequencies, zero-point and thermal energy corrections, and force constants were calculated. The standard temperature (298.15 K) and pressure (1 atm) were used to obtain Gibbs free energies. The natural population analysis has been made by using the natural bond orbital (NBO).[79,80]

As we mentioned before, energy surface crossings play important roles in understanding chemical reactivity when a process involves a change in the total electronic spin. Determining the lowest CP at which two energy surfaces corresponding to different spin states intersect with minimum energy is fundamental because it serves as the most likely place where the transition occurs.[55,81−83] To localize and characterize the CPs, the concept of minimum energy crossing point (MECP) on the seam line at which two electronic surfaces of different spin multiplicities intersect has been used. Therefore, all coordinates were optimized in searches for the CPs between the two PESs in which DFT energies and gradients were

(65) Mercero, J. M.; Matxain, J. M.; Lopez, X.; York, D. M.; Largo, A.; Eriksson, L. A.; Ugalde, J. M. *Int. J. Mass Spectrom.* **2005**, *240*, 37−99.
(66) Gracia, L.; Sambrano, J. R.; Safont, V. S.; Calatayud, M.; Beltrán, A.; Andres, J. *J. Phys. Chem. A* **2003**, *107*, 3107−3120.
(67) Gracia, L.; Andres, J.; Sambrano, J. R.; Safont, V. S.; Beltrán, A. *Organometallics* **2004**, *23*, 730−739.
(68) Frisch, M. J.; Trucks, G. W.; Schlegel, H. B.; Scuseria, G. E.; Robb, M. A.; Cheeseman, J. R.; Montgomery, J., J. A.; Vreven, T.; Kudin, K. N.; Burant, J. C.; Millam, J. M.; Iyengar, S. S.; Tomasi, J.; Barone, V.; Mennucci, B.; Cossi, M.; Scalmani, G.; Rega, N.; Petersson, G. A.; Nakatsuji, H.; Hada, M.; Ehara, M.; Toyota, K.; Fukuda, R.; Hasegawa, J.; Ishida, M.; Nakajima, T.; Honda, Y.; Kitao, O.; Nakai, H.; Klene, M.; Li, X.; Knox, J. E.; Hratchian, H. P.; Cross, J. B.; Adamo, C.; Jaramillo, J.; Gomperts, R.; Stratmann, R. E.; Yazyev, O.; Austin, A. J.; Cammi, R.; Pomelli, C.; Ochterski, J. W.; Ayala, P. Y.; Morokuma, K.; Voth, G. A.; Salvador, P.; Dannenberg, J. J.; Zakrzewski, V. G.; Dapprich, S.; Daniels, A. D.; Strain, M. C.; Farkas, O.; Malick, D. K.; Rabuck, A. D.; Raghavachari, K.; Foresman, J. B.; Ortiz, J. V.; Cui, Q.; Baboul, A. G.; Clifford, S.; Cioslowski, J.; Stefanov, B. B.; Liu, G.; Liashenko, A.; Piskorz, P.; Komaromi, I.; Martin, R. L.; Fox, D. J.; Keith, T.; Al-Laham, M. A.; Peng, C. Y.; Nanayakkara, A.; Challacombe, M.; Gill, P. M. W.; Johnson, B.; Chen, W.; Wong, M. W.; Gonzalez, C.; Pople, J. A. *Gaussian03 (Revision B.04)*; Gaussian, Inc.: Pittsburgh, PA, 2003.
(69) Lee, C.; Yang, R. G.; Parr, R. G. *Phys. Rev. B* **1988**, *37*, 785−789.
(70) Becke, A. D. *J. Chem. Phys.* **1993**, *98*, 5648−5652.
(71) Stephens, P. J.; Devlin, F. J.; Chabalowski, C. F.; Frisch, M. J. *J. Phys. Chem.* **1994**, *98*, 11623.
(72) Pople, J. A.; Headgordon, M.; Raghavachari, K. *J. Chem. Phys.* **1987**, *87*, 5968−5975.
(73) Sambrano, J. R.; Andrés, J.; Gracia, L.; Safont, V. S.; Beltrán., A. *Chem. Phys. Lett.* **2004**, *384*, 56−62.
(74) Schlegel, H. B. *J. Comput. Chem.* **1982**, *3*, 214−218.
(75) McIver, J. W., Jr. *Acc. Chem. Res.* **1974**, *7*, 72−77.
(76) Fukui, K. *J. Phys. Chem.* **1970**, *74*, 4161−4163.
(77) González, C.; Schlegel, H. B. *J. Chem. Phys.* **1989**, *90*, 2154−2161.
(78) González, C.; Schlegel, H. B. *J. Phys. Chem.* **1990**, *94*, 5523−5527.
(79) Reed, A. E.; Weinstock, R. B.; Weinhold, F. *J. Chem. Phys.* **1985**, *83*, 735−746.
(80) Reed, A. E.; Curtiss, L. A.; Weinhold, F. *Chem. Rev.* **1988**, *88*, 899−926.
(81) Armentrout, P. B. *Science* **1991**, *251*, 175−179.
(82) Yarkony, D. R. *Rev. Mod. Phys.* **1996**, *68*, 985−1013.
(83) Plattner, D. *Angew. Chem., Int. Ed.* **1999**, *38*, 82−86.

calculated for each spin multiplicity. Starting from the TS closest to the crossing seams, the reaction pathway was traced down to the corresponding minimum. Thereafter, each optimized point along the IRC path was submitted to a single-point energy calculation with the other electronic state. In this way, we obtain the CPs as the structures that have identical geometry and energy in the s and t states. This procedure has been used in our previous studies.[66,67,73] For the sake of comparison, the mathematical algorithm to MECPs developed by Harvey et al.[53] has also been employed. The CPs that we obtain in this way can be considered as estimates of the MECPs between s and t hypersurfaces.

3. Results and Discussion

A detailed analysis of the reactive PES associated with the reaction of VO_2^+ ($^1A_1/^3A''$) with propene renders the presence of two different reactive channels, associated with dehydrogenation (*Deh*) and oxidation (*Ox*) processes, and both processes may have three possible reaction pathways to obtain (i) $V(OH)_2^+$ ($^1\Sigma^+/^3\Sigma^-$) and allene (*path Deh1*), (ii) $V(OH)_2^+$ ($^1\Sigma^+/^3\Sigma^-$) and propyne (*path Deh2*), (iii) VO_2^+ ($^1A_1/^3A''$), H_2, and allene (*path Deh3*), (iv) VO^+ ($^1\Delta/^3\Sigma$) and acetone (*path Ox1*), (v) VO^+ ($^1\Delta/^3\Sigma$) and propanaldehyde (*path Ox2*), and (vi) VO^+ ($^1\Delta/^3\Sigma$), H_2, and propenaldehyde (*path Ox3*). The selected geometrical parameters of the stationary points at the singlet electronic state are presented in Figures 1a and 1b for the dehydrogenation and oxygenation processes, respectively, while the corresponding stationary points at the triplet electronic state are presented in Figures 2a and 2b, respectively. The Gibbs free energy profiles are shown in Figures 3a and 3b for the dehydrogenation and oxygenation processes, respectively. In Table 1 the results of the natural population analysis are reported.

The most stable combination of reactants is formed by **s-VO_2^+** ($^1A_1$) and C_3H_6 (^1A), thus belonging to the overall singlet PES. The triplet state combination **t-VO_2^+** ($^3A''$) and **C_3H_6** (^1A) stands 35.6 kcal/mol above the singlet. For the products, the most stable combination is **t-$V(OH)_2^+$** ($^3\Sigma^-$) and allene for the *path Deh1*, **t-$V(OH)_2^+$** ($^3\Sigma^-$) and propyne for *path Deh2*, **s-VO_2^+** ($^1A_1$), H_2, and allene for the *path Deh3*, **t-VO^+** ($^3\Sigma$) and acetone for *path Ox1*, **t-VO^+** ($^3\Sigma$) and propanaldehyde for *path Ox2*, and **t-VO^+** ($^3\Sigma$), H_2, and propenaldehyde for the *path Ox3*. Four of these six reactive channels (*paths Deh1*, *Deh2*, *Ox1*, and *Ox2*) correspond to exergonic processes, $\Delta G = -24.9$, -23.1, -18.2, and -9.5 kcal/mol, respectively. In the four processes $V(OH)_2^+$ or VO^+ products are obtained as a triplet ground electronic state; then, it is obvious that from the most stable reactants to the most stable products, at least one CP must take place.

An analysis of the results (see Figure 3) shows that four reactant complexes, at both s and t electronic states for the initial addition processes, have been localized and their formation proceeds without any barrier: **s/t-1V**, **s/t-1O**, **s/t-2V**, and **s/t-3V**, for the s and t electronic states, respectively. The formation of all reactant complexes produces a large amount of exothermic energy, and it is associated with spontaneous processes. VO_2^+ preferably attacks the terminal C_1 carbon atom of propene to form **s/t-1V**, while the interaction of the V atom of the vanadyl moiety with the central C_2 carbon atom of the propene fragment renders **s/t-2V** and **s/t-3V** complexes. However, along the oxidation processes at the s and t electronic states, the reaction complex implies the formation of a three-membered ring between the O atom of the VO_2^+ moiety and the two carbon atoms, C_1 and C_2, **s/t-1O**. Therefore, the addition of the vanadyl cation to the propene molecule is likely to be the starting point for the reaction, and this interaction decides whether the pathway will go through three dehydrogenation processes, *paths Deh1*, *Deh2*, and *Deh3*, or three oxidation processes, *paths Ox1*, *Ox2*, and *Ox3*.

s-1V is the most stable reactant complex for the dehydrogenation process, with geometric parameters similar to the separated reactants, except that the C_1-C_2 bond is slightly elongated to 1.376 Å compared with 1.327 Å in free propene. **t-1O** is the most stable addition complex for the oxidation process, with **s-1V** being 15.4 kcal/mol more stable than **t-1O**. Along the oxygenation channels, the triplet state, **t-1O**, is 24.3 kcal/mol more stable than the singlet, **s-1O**. Then, the first CP, **CP-*Ox***, along the oxidation processes occurs at this stage. The geometry of **CP-*Ox*** is depicted in Figure 4. An analysis of the corresponding values shows that **CP-*Ox*** is geometrically and energetically closer to **s-1O** than to **t-1O**, although both reactant complexes (**s-1O** and **t-1O**) are rather similar. For comparison purposes, we have also used the algorithm proposed by Harvey et al.[53] to characterize the MECP, and the corresponding geometrical values are also presented in Figure 4. Total energy values of the **CP-*Ox*** and the MECP related to the singlet reactants are 12.6 and 14.3 kcal/mol, respectively, and those related to **t-1O** are 29.5 and 27.2 kcal/mol, respectively.

Therefore, only **s-1V** and **t-1O** open the door for the dehydrogenation and oxidation channels, respectively. In **s/t-1V**, the negative charge of this C_1 atom increases 0.26 and 0.31 au, respectively, and a noticeable electronic charge transfer takes place from the propene fragment to the vanadyl moiety (0.28 and 0.22 au, respectively). In **s/t-1O**, however, the negative charge of both C_1 and C_2 atoms decreases around 0.32 au and an electronic charge transfer takes place from the propene fragment to the vanadyl moiety, 0.40 and 0.43 au, respectively.

Dehydrogenation Processes. *Path Deh1*. From **s/t-1V**, the next step is associated with a hydrogen transfer process between the C_3 atom and the O_2 atom of the vanadyl cation, to yield the **s/t-2-D1** intermediates, via six-membered transition states, **s/t-TS1-D1**. These transition structures are situated energetically near the entrance channel, and the activation free energies are 26.4/8.6 kcal/mol, respectively, while the formation of **s/t-2-D1** is quite exothermic, 47.7 and 48.7 kcal/mol, respectively. These intermediates, **s/t-2-D1**, present a pyramidal structure between the V atom and the three C atoms, and they are the global minima on the corresponding PESs. From **s/t-2-D1** another hydrogen migration takes place along **s/t-TS2-D1**, from the central carbon atom, C_2, to the other oxygen atom, O_1, of the vanadyl fragment, to render the product complexes **s/t-3-D1**, being also very stable intermediates. Finally the separated products, **s/t-$V(OH)_2^+$** + allene, can be obtained directly from **s/t-3-D1** product complexes, overcoming a barrier height of 47.9/35.0 kcal/mol, respectively. Both TSs, **s/t-TS1-D1** and **s/t-TS2-D1**, are associated with an activation of C−H bonds of the propene moiety, and they can be considered as consecutive hydrogen transfer processes (the hydrogen atoms being transferred, H_1 and H_2, are positively charged, in the range 0.38−0.50 au); therefore, high values of imaginary vibrational frequencies (1495i and 940i cm^{-1} for the s state, 1034 and 1642i cm^{-1} for the t state) are found. The **t-TS2-D1** is 18.1 kcal/mol more stable than **s-TS2-D1**; therefore the crossing point, **CP-*Deh1***, between s and t states takes place just before this second hydrogen transfer process, and its existence opens the possibility for an intersystem crossing between s and t electronic states. Therefore, from **s-2-D1**, the reactive channel taking place at the triplet state is energetically favorable via **CP-*Deh1***, to follow with **t-TS2-D1** and the product complex **t-3-D1**, and finally to obtain the most stable combination of products, **t-$V(OH)_2^+$** and

Table 1. Natural Population Analysis for the Stationary Points: (a) Singlet State and (b) Triplet State[a]

(a)

	V	O_1	O_2	C_1	C_2	C_3	H_1	H_2	H_3	H_4	H_5	H_6
s-VO_2^+	1.60	−0.30	−0.30									
s-propene				−0.38	−0.16	−0.59	0.20	0.18	0.18	0.18	0.19	0.20
s-1V	1.49	−0.38	−0.39	−0.64	0.08	−0.64	0.26	0.23	0.25	0.24	0.23	0.27
s-TS1-D1	1.52	−0.35	−0.61	−0.67	0.02	−0.54	0.42	0.22	0.26	0.24	0.25	0.25
s-2-D1	1.53	−0.34	−0.81	−0.51	−0.12	−0.51	0.52	0.25	0.24	0.25	0.24	0.25
s-TS2-D1	1.54	−0.63	−0.81	−0.50	−0.10	−0.51	0.53	0.50	0.24	0.25	0.24	0.25
s-3-D1	1.60	−0.83	−0.83	−0.53	−0.12	−0.31	0.53	0.53	0.25	0.25	0.22	0.24
s-TS1-D3	1.46	−0.34	−0.78	−0.66	0.14	−0.37	0.52	−0.07	0.27	0.28	0.27	0.28
s-2-D3	1.34	−0.31	−0.74	−0.39	−0.00	−0.41	0.52	−0.11	0.27	0.27	0.26	0.29
s-TS2-D3	1.32	−0.32	−0.50	−0.34	−0.08	−0.34	0.32	−0.10	0.25	0.27	0.25	0.27
s-3-D3	1.38	−0.37	−0.36	−0.71	0.25	−0.40	0.05	0.04	0.26	0.27	0.28	0.28
s-4-D3	1.50	−0.37	−0.37	−0.43	−0.03	−0.38			0.27	0.28	0.25	0.28
s-TS1-D2	1.35	−0.35	−0.63	−0.59	0.10	−0.62	0.25	0.49	0.24	0.27	0.25	0.25
s-2-D2	1.50	−0.35	−0.77	−0.49	0.01	−0.64	0.26	0.52	0.28	0.20	0.24	0.25
s-TS2-D2	1.43	−0.52	−0.80	−0.43	0.01	−0.65	0.25	0.52	0.40	0.28	0.25	0.26
s-3-D2	1.53	−0.79	−0.79	−0.36	0.01	−0.65	0.25	0.52	0.52	0.26	0.25	0.25
s-Allene				−0.47	0.09	−0.47			0.21	0.21	0.21	0.21
s-propyne				−0.25	0.00	−0.63	0.22			0.22	0.22	0.22
s-$V(OH)_2^+$	1.80	−0.93	−0.93				0.53	0.53				
s-1O	1.39	−0.69	−0.52	−0.03	0.16	−0.62	0.22	0.21	0.20	0.21	0.22	0.21
s-TS1-O1	1.37	−0.75	−0.50	0.00	0.04	−0.56	0.22	0.31	0.23	0.22	0.22	0.21
s-2-O1	1.44	−0.72	−0.53	−0.67	0.67	−0.67	0.26	0.25	0.23	0.25	0.24	0.24
s-Acetone		−0.55		−0.67	0.61	−0.67	0.22	0.21	0.22	0.21	0.21	0.21
s-VO^+	1.45		−0.45									
s-TS1-O2	1.31	−0.78	−0.52	−0.03	0.14	−0.67	0.25	0.23	0.31	0.24	0.25	0.23
s-2-O2	1.44	−0.68	−0.51	0.51	−0.48	−0.56	0.23	0.23	0.25	0.17	0.21	0.20
s-propanaldehyde		−0.52		0.46	−0.47	−0.56	0.19	0.21	0.21	0.09	0.20	0.19
s-TS1-O3	1.36	−0.66	−0.63	0.36	−0.40	−0.58	0.23	0.53	0.25	0.20	0.21	0.23
s-2-O3	1.56	−0.58	−0.86	0.16	−0.34	−0.61	0.23	0.52	0.23	0.22	0.23	0.24
s-TS2-O3	1.31	−0.55	−0.77	0.17	−0.25	−0.44	0.02	0.52	0.24	0.22	0.25	0.28
s-3-O3	1.40	−0.81	−0.65	0.42	−0.32	−0.13	−0.25	0.52	0.23	0.18	0.20	0.22
s-TS3-O3	1.33	−0.67	−0.61	0.44	−0.34	−0.13	−0.20	0.35	0.24	0.18	0.19	0.22
s-4-O3	1.29	−0.68	−0.43	0.46	−0.33	−0.14	−0.02	0.02	0.23	0.18	0.19	0.22
s-5-O3	1.47	−0.71	−0.63	0.43	−0.34	−0.16			0.23	0.18	0.19	0.21
s-propenaldehyde		−0.52		0.40	−0.28	−0.28			0.21	0.10	0.18	0.19

(b)

	V	O_1	O_2	C_1	C_2	C_3	H_1	H_2	H_3	H_4	H_5	H_6
t-VO_2^+	1.61	−0.32	−0.28									
t-1V	1.49	−0.33	−0.37	−0.62	0.01	−0.63	0.25	0.23	0.25	0.24	0.23	0.27
t-TS1-D1	1.52	−0.35	−0.61	−0.67	0.02	−0.54	0.42	0.22	0.26	0.24	0.25	0.25
t-2-D1	1.51	−0.41	−0.89	−0.30	−0.32	−0.30	0.51	0.26	0.22	0.24	0.22	0.24
t-TS2-D1	1.52	−0.59	−0.88	−0.12	−0.39	−0.37	0.51	0.38	0.22	0.23	0.24	0.25
t-3-D1	1.56	−0.81	−0.83	−0.56	0.14	−0.56	0.53	0.53	0.25	0.26	0.25	0.26
t-TS1-D3	1.52	−0.41	−0.88	−0.27	−0.43	−0.15	0.52	0.21	0.21	0.24	0.22	0.23
t-2-D3	1.34	−0.34	−0.77	−0.47	−0.01	−0.18	0.52	−0.14	0.27	0.28	0.24	0.25
t-TS2-D3	1.28	−0.32	−0.51	−0.40	−0.07	−0.21	0.32	−0.12	0.27	0.27	0.24	0.25
t-3-D3	1.35	−0.36	−0.37	−0.30	−0.07	−0.33	0.03	0.06	0.25	0.26	0.24	0.25
t-4-D3	1.45	−0.40	−0.40	−0.20	−0.04	−0.45			0.25	0.25	0.26	0.27
t-TS1-D2	1.56	−0.41	−0.61	−0.55	0.04	−0.64	0.27	0.32	0.24	0.26	0.25	0.26
t-2-D2	1.59	−0.43	−0.86	−0.70	0.27	−0.70	0.26	0.51	0.26	0.26	0.26	0.28
t-TS2-D2	1.48	−0.57	−0.89	−0.55	0.18	−0.67	0.28	0.51	0.37	0.31	0.26	0.29
t-3-D2	1.60	−0.90	−0.90	−0.32	0.05	−0.66	0.25	0.52	0.52	0.29	0.25	0.27
t-$V(OH)_2^+$	1.76	−0.91	−0.91				0.53	0.53				
t-1O	1.40	−0.70	−0.54	−0.02	0.16	−0.63	0.22	0.22	0.20	0.22	0.25	0.22
t-TS1-O1	1.48	−0.78	−0.51	−0.05	0.05	−0.58	0.22	0.31	0.23	0.20	0.22	0.22
t-2-O1	1.40	−0.72	−0.54	−0.67	0.71	−0.72	0.26	0.25	0.24	0.26	0.25	0.24
t-VO^+	1.46		−0.46									
t-TS1-O2	1.37	−0.84	−0.61	−0.10	0.26	−0.70	0.32	0.22	0.31	0.30	0.28	0.25
t-2-O2	1.40	−0.69	−0.53	0.57	−0.49	−0.55	0.21	0.23	0.26	0.17	0.23	0.21
t-TS1-O3	1.48	−0.70	−0.68	0.38	−0.42	−0.58	0.23	0.42	0.25	0.19	0.21	0.23
t-2-O3	1.60	−0.63	−0.91	0.18	−0.30	−0.60	0.23	0.52	0.23	0.21	0.22	0.24
t-TS2-O3	1.38	−0.55	−0.84	0.37	−0.39	−0.26	−0.17	0.51	0.26	0.20	0.23	0.25
t-3-O3	1.46	−0.70	−0.86	0.48	−0.32	−0.12	−0.28	0.52	0.24	0.17	0.20	0.22
t-TS3-O3	1.38	−0.71	−0.63	0.50	−0.33	−0.13	0.34	0.24	0.24	0.19	0.19	0.23
t-4-O3	1.33	−0.51	−0.71	0.49	−0.34	−0.12	0.02	0.02	0.23	0.17	0.20	0.22
t-5-O3	1.43	−0.72	−0.55	0.48	−0.34	−0.12			0.23	0.17	0.20	0.22

[a] The calculated charge (au) on the indicated atoms is reported at the B3LYP/6-311G(2d,p) level.

allene. The geometry of the **CP-*Deh1*** is depicted in Figure 4. An analysis of the corresponding values shows that **CP-*Deh1*** is in a geometric and energetic middle position between **s-TS2-D1** and **t-TS2-D1**. For comparison purposes, the characterized MECP using the algorithm proposed by Harvey et al. is also presented in Figure 4. It is important to note that similar values of the geometrical parameters and relative energies are found, although geometrical values of the **CP-*Deh1*** are close to the

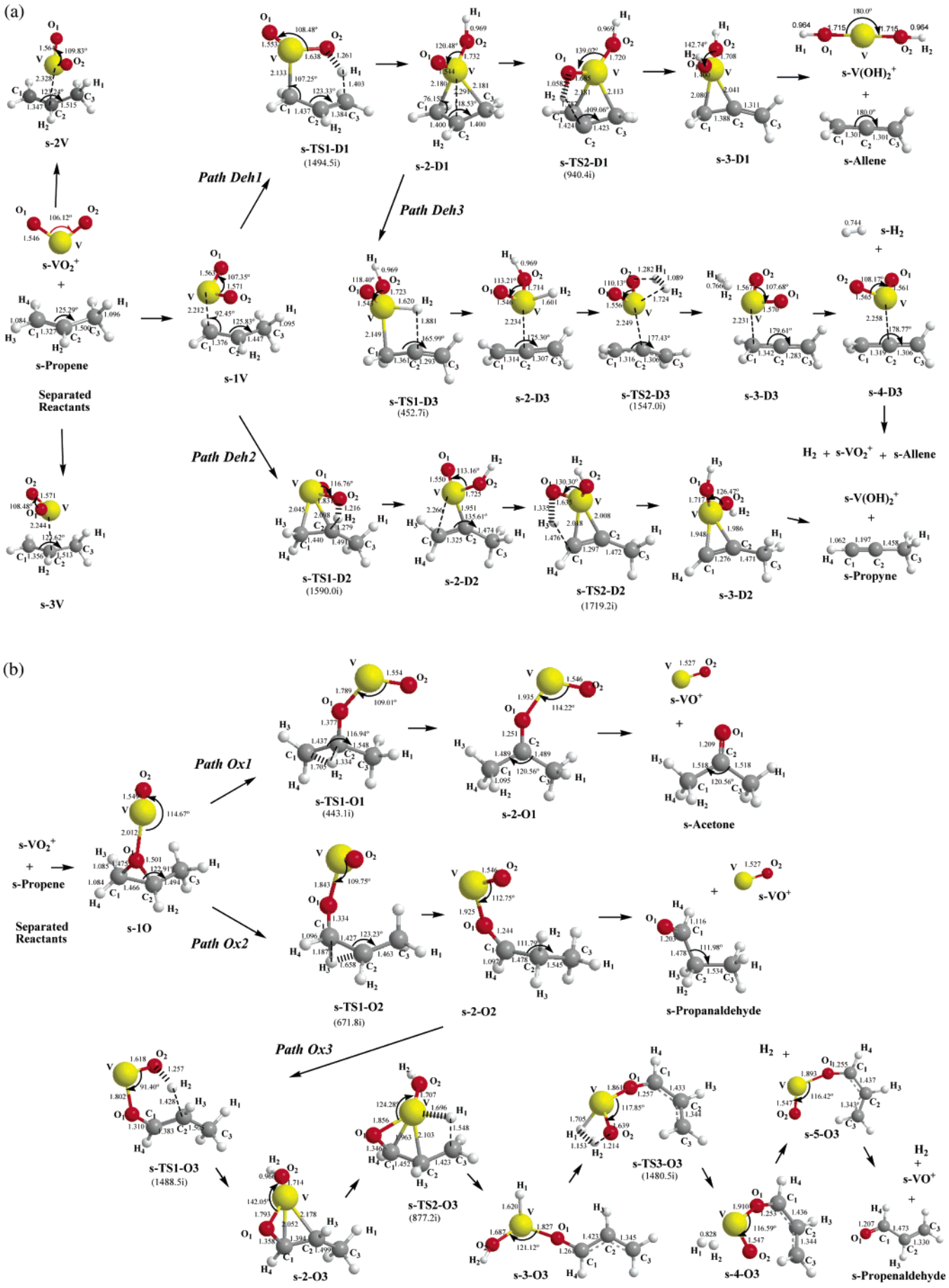

Figure 1. Structures (distances in Å and angles in deg) of the stationary points found at the B3LYP/6-311G(2d,p) level for the singlet state. For TSs, the imaginary vibrational frequencies (cm^{-1}) are shown in italics. (a) Dehydrogenation processes. (b) Oxygenation processes.

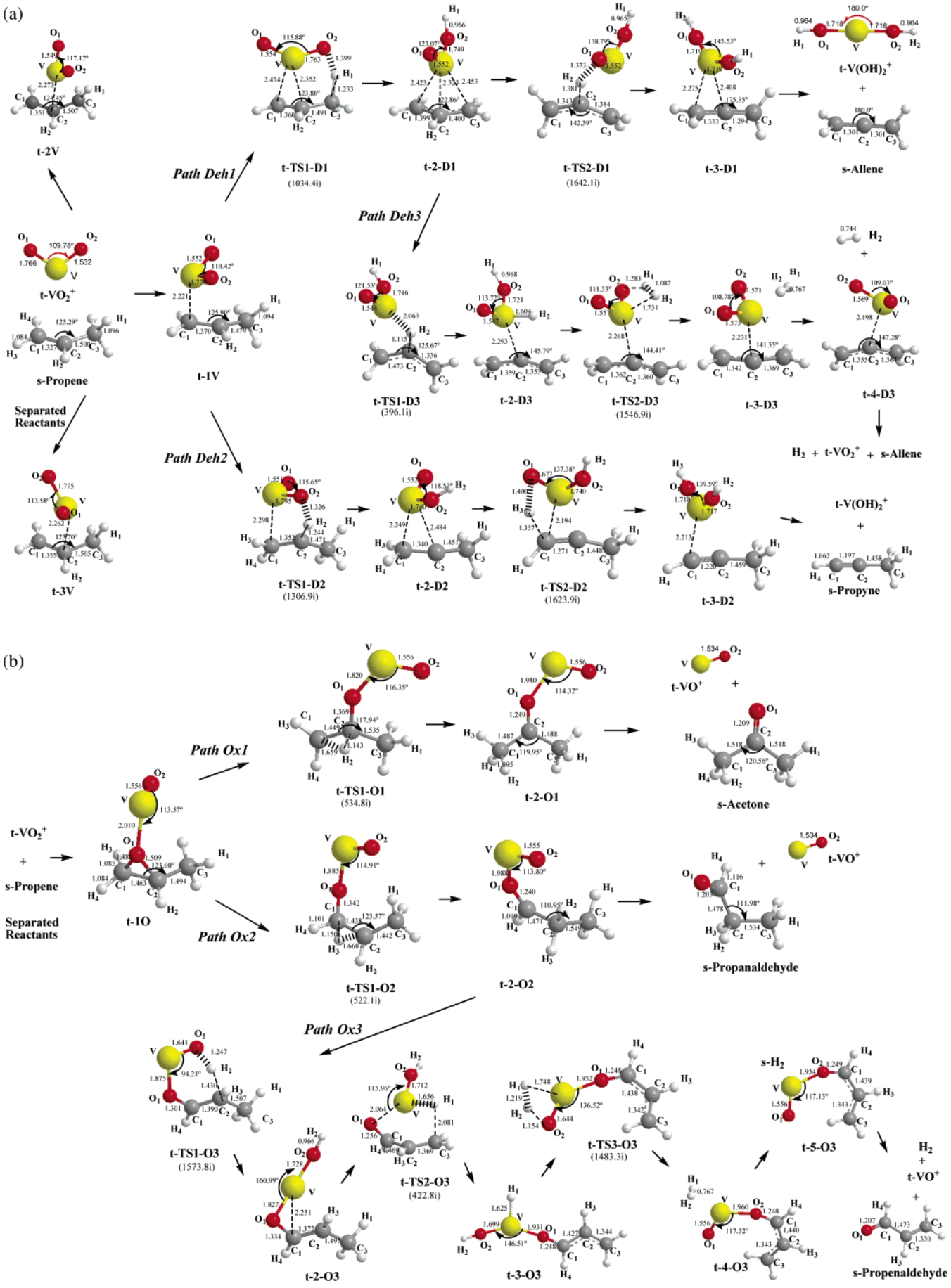

Figure 2. Structures (distances in Å and angles in deg) of the stationary points found at the B3LYP/6-311G(2d,p) level for the triplet state. For TSs, the imaginary vibrational frequencies (cm^{-1}) are shown in italics. (a) Dehydrogenation processes. (b) Oxygenation processes.

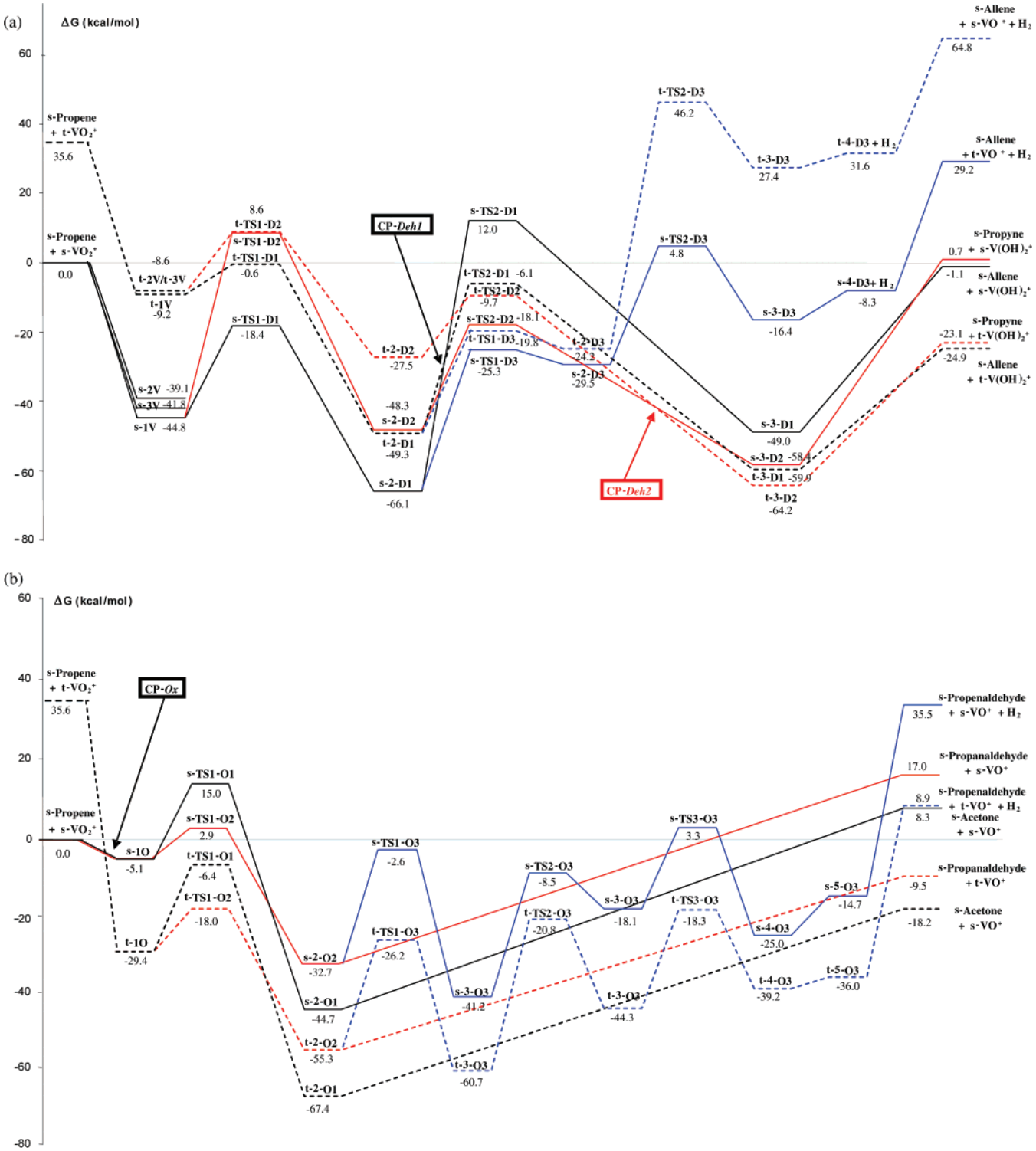

Figure 3. Gibbs free energy profile, relative to the reactants at the singlet state. The total Gibbs free energy value for the separated reactants is −1212.087871 hartrees at the B3LYP/6-311G(2d,p) level. The singlet state is depicted as solid lines and the triplet state as dashed lines. (a) Dehydrogenation processes, *path Deh1* in black, *path Deh2* in red, and *path Deh3* in blue. (b) Oxygenation processes, *path Ox1* in black, *path Ox2* in red, and *path Ox3* in blue.

s-TS2-D1 and the corresponding data of the MECP are closer to those of **t-TS2-D1** than to **s-TS2-D1**. The O_1-H_2 distance is 1.058 Å (1.373 Å) in **s-TS2-D1** (**t-TS2-D1**) and 1.184 Å (1.294 Å) in **CP-*Deh1*** (MECP). Also, the H_2-C_2 distance is 1.787 Å (1.381 Å) in **s-TS2-D1** (**t-TS2-D1**) and 1.423 Å (1.391 Å) in **CP-*Deh1*** (MECP). This parallelism can be sensed also in the C_1-C_2 or C_2-C_3 distances. Total energy values of the **CP-*Deh1*** and the MECP related to **s-2-D1** are 43.0 and 46.1 kcal/mol, respectively, and those related to **t-TS2-D1** are 23.2 and 20.1 kcal/mol, respectively.

Path Deh2. From **s/t-1V**, the next step is associated with a hydrogen transfer between the central carbon atom, C_2, to the O_2 atom of the vanadyl cation, to yield the **s/t-2-D2** intermediates, via five-membered transition states, **s/t-TS1-D2**. The activation free energy is 53.4/17.8 kcal/mol, respectively (although **s/t-TS1-D2** present similar energetic values), while

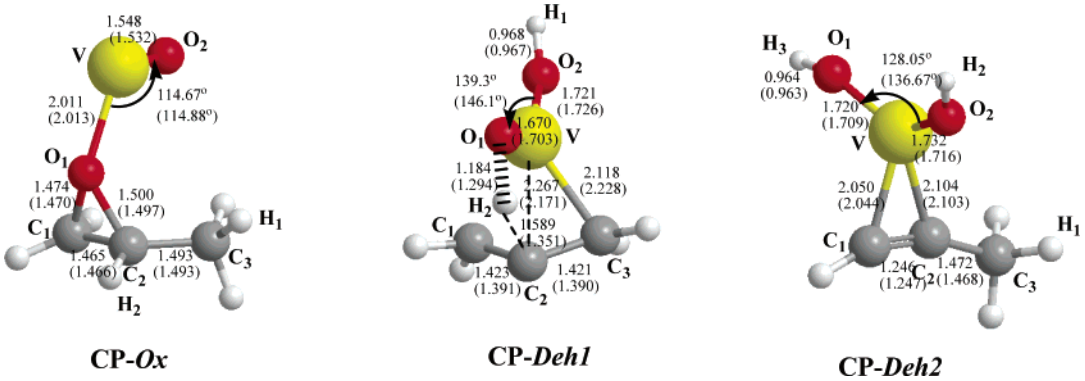

Figure 4. Structure of the crossing points, **CP-*Deh1***, **CP-*Deh2***, and **CP-*Ox***, found at the B3LYP/6-311G(2d,p) level (in parentheses are presented corresponding values using the algorithm proposed by Harvey et al.[53] to characterize the MECP).

the formation of **s/t-2-D2** is quite exothermic, 56.9 and 36.1 kcal/mol, respectively. The next step from **s/t-2-D2** to the product complexes **s/t-3-D2** takes place along **s/t-TS2-D2**, associated with another hydrogen migration from the C_1 atom to the other oxygen atom, O_1, of the vanadyl fragment. Finally, from **s/t-3-D2** product complexes, the separated products, **s/t-V(OH)$_2^+$** and propyne, can be directly obtained surmounting a barrier height of 59.1/41.1 kcal/mol, respectively. Both TSs, **s/t-TS1-D2** and **s/t-TS2-D2**, are also considered as consecutive hydrogen transfer processes (the hydrogen atoms being transferred, H_2 and H_3, are positively charged, in the range 0.32−0.49 au). Then, values similar to the TSs along the *path Deh1* are calculated for the corresponding imaginary vibrational frequencies (1590i and 1719i cm^{-1} for the s state, 1307 and 1624i cm^{-1} for t state). The **s-TS2-D2** is 8.4 kcal/mol more stable than **t-TS2-D2**, while the product complex **t-3** is 5.8 kcal/mol more stable than **s-3**; therefore the crossing point, **CP-*Deh2***, between the s and t states takes place just after this second hydrogen transfer process. Consequently, from **s-TS2-D2**, the reactive channel taking place at the triplet state is energetically favorable via **CP-*Deh2***, to follow with the product complex **t-3-D2**, and finally to obtain the most stable combination of products, **t-V(OH)$_2^+$** and propyne. The geometry of **CP-*Deh2*** and that corresponding to the MECP are also depicted in Figure 4, both with geometric and energetic middle positions between **s-3-D2** and **t-3-D2** minima. The C_1-C_2 distance is 1.276 Å (1.220 Å) in **s-3-D2** (**t-3-D2**) and 1.246 Å (1.247 Å) in **CP-*Deh2*** (MECP). Also, the C_1-V distance is 1.948 Å (2.213 Å) in **s-3-D2** (**t-3-D2**) and 2.050 Å (2.044 Å) in **CP-*Deh2*** (MECP). Other values such as the angle O_1-V-O_2 is 128.05° (136.67°) in **CP-*Deh2*** (MECP) and 126.47° (139.59°) in **s-3-D2** (**t-3-D2**). Total energy values of the **CP-*Deh2*** and the corresponding MECP related to the **s-TS2-D2** are 36.5 and 38.9 kcal/mol, respectively, and those related to the **t-3-D2** are 7.3 and 5.9 kcal/mol, respectively.

Path Deh3. From the minima **s/t-2-D1** (obtained in the second step of the *path Deh1*) it is possible to continue the reaction with a step associated with a second hydrogen transfer process, **s/t-TS1-D3**, between the central carbon atom, C_2, and the vanadium atom to render the minima **s/t-2-D3**. Therefore, these transition structures, **s/t-TS1-D3**, present low values of imaginary vibrational frequencies, 453i/396i cm^{-1}, respectively, and the hydrogen atom being transferred, H_2, is −0.07 au negatively charged. The activation free energy is 40.8/29.5 kcal/mol, respectively, while the formation of **s/t-2-D3** is rather exothermic, 4.2/4.4 kcal/mol, respectively. The next step from **s/t-2-D3** to the product complexes **s/t-3-D3** takes place along **s/t-TS2-D3**, associated with hydrogen migrations from the O_2 atom of the vanadyl moiety to the hydrogen just joined at the vanadium, H_2. Therefore, these transition structures, **s/t-TS2-D3**, present high values of imaginary frequencies (1547i cm^{-1}), and the charge on the transferred hydrogen atoms is negative, −0.10/-0.12 au, respectively. At **s/t-3-D3**, the formed hydrogen molecule is interacting still with the vanadyl moiety (these hydrogen atoms are ∼0.05 au positively charged), so from **s/t-3-D3** product complexes, the separated fragments, **H_2** and **s/t-4-D3**, can be directly obtained, overcoming a low energy barrier of 8.1/4.2 kcal/mol, respectively. Finally, from **s/t-4-D3**, the separated products, **s/t-VO_2^+** and allene, can be directly yielded, surmounting barrier heights of 37.5 and 33.2 kcal/mol. Therefore, along this path no spin inversion process takes place and the singlet state is preferred.

Oxidation Processes. *Path Ox1 and Path Ox2*. **s/t-1O** open two alternative oxidation processes. Along *path Ox1* there is an intermolecular hydrogen transfer, H_2, from C_2 to C_1 carbon atoms, via **s/t-TS1-O1**, to obtain the product complexes **s/t-2-O1**, where the oxygen atom, O_1, of the vanadyl moiety is linked to the C_2 atom. This intermediate is the global minimum on the corresponding PESs. An opposite trend is found along the *path Ox2*; the hydrogen transfer process, H_3, takes place from C_1 to C_2 carbon atoms, via **s/t-TS1-O2**, with the formation of the product complexes, **s/t-2-O2**. In this case the oxygen atom, O_1, of the vanadyl moiety is linked to the terminal C_1 atom. Transition structures, **s/t-TS1-O1** and **s/t-TS1-O2**, of *path Ox1* and *path Ox2*, are situated energetically above the entrance channel, 15.0 and 2.9 kcal/mol, respectively, and they present low values of imaginary vibrational frequencies, 443i/535i and 672i/522i cm^{-1}, respectively. These values can be justified due to the hydrogen transfer that takes place between adjacent carbon atoms, and the hydrogen atom being transferred is 0.31 au positively charged. From **s/t-TS1-O1**, **s/t-2-O1** product complexes are formed, overcoming an activation free energy (9.9/23.0 kcal/mol, respectively), while the formation of **s/t-2-O1** is quite exothermic, 59.7 and 61.0 kcal/mol, respectively. Finally acetone and the **t-VO$^+$** cation can be rendered, surmounting a barrier height of 49.2 kcal/mol from **t-2-O1**. From **s/t-TS1-O2**, **s/t-2-O2** product complexes are formed, overcoming lower barriers of 8.0/11.4 kcal/mol, respectively, while the formation of **s/t-2-O2** is less exothermic than in *path Ox1*, 35.6 and 37.3 kcal/mol, respectively. Finally propanaldehyde and the **t-VO$^+$** cation can be obtained climbing up a barrier height of 45.8 kcal/mol from **t-2-O2**.

Path Ox3. From the minima **s/t-2-O2** (obtained in the second step of the *path Ox2*) it is possible to continue the reaction with a step associated with a second hydrogen transfer process (intermolecular), **s/t-TS1-O3**, between the central carbon atom, C_2, and the O_2 atom to render the minima **s/t-2-O3**. These transition structures, **s/t-TS1-O3**, present high values of imagi-

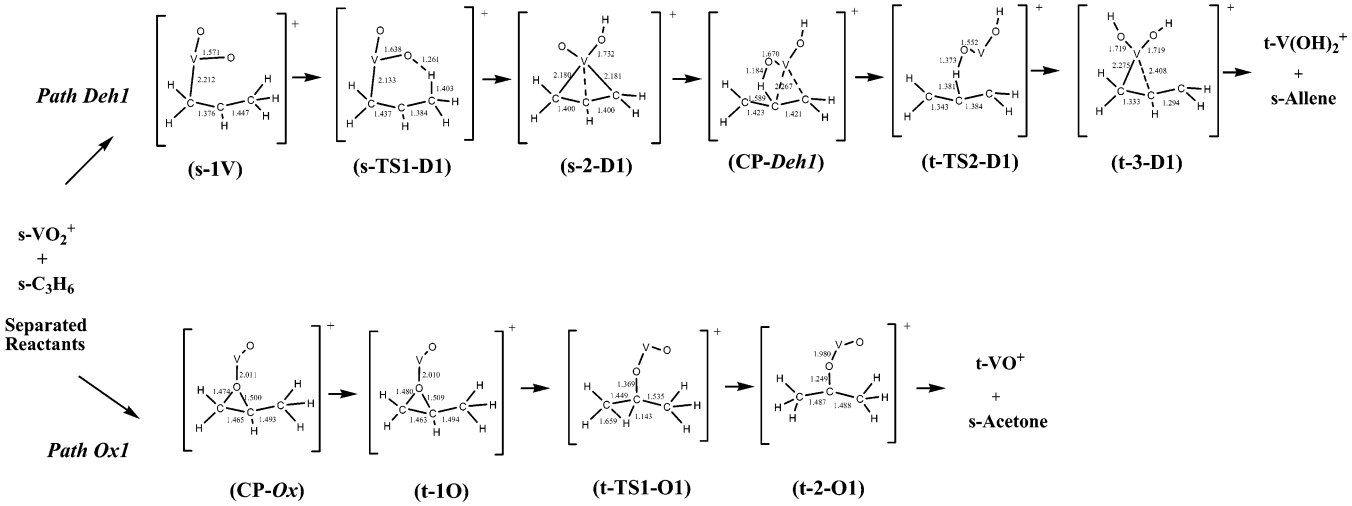

Figure 5. Structure of stationary points and crossing points along the most favorable reaction pathways for the dehydrogenation process, *path Deh1*, and for the oxygenation process, *path Ox1*.

nary vibrational frequencies, 1489i/1574i cm^{-1}, respectively, and the hydrogen atom being transferred, H_2, is 0.53/0.42 au positively charged. The activation free energies are 30.1/29.1 kcal/mol, respectively, while the formation of **s/t-2-O3** is rather exothermic, 38.6/34.5 kcal/mol, respectively. The next step from **s/t-2-O3** to the global minima on PESs, **s/t-3-O3**, takes place along **s/t-TS2-O3**, corresponding to hydrogen transfer processes between the terminal carbon atom, C_3, and the vanadium atom with low values of imaginary vibrational frequencies, 877i/423i cm^{-1}, respectively, and the hydrogen atom being transferred, H_1, is 0.02/−0.17 au charged. From **s/t-3-O3** minima, hydrogen migrations from the O_2 atom of the vanadyl moiety to the hydrogen just joined at the vanadium, H_1, take place. Therefore, these transition structures, **s/t-TS3-O3**, present high values of imaginary frequencies (1480i/1483i cm^{-1}, respectively). The charge of the hydrogen atom being transferred, H_2, decreases 0.17/0.28 au, respectively. From this step, **s/t-4-O3** product complexes are rendered, where the formed hydrogen molecule is interacting still with the vanadyl moiety (the hydrogen atoms forming the H_2 fragment are ∼0.02 au charged). So from **s/t-4-O3** product complexes, the separated fragments, H_2 and **s/t-5-O3**, can be directly obtained, overcoming a low energy barrier of 10.3/3.2 kcal/mol, respectively. Finally, from **s/t-5-O3** product complexes, the separated products, H_2 molecule, **s/t-VO**$^+$, and propenaldehyde, can be directly yielded, surmounting barrier heights of 50.2 and 44.9 kcal/mol. Furthermore, spin restrictions do not play a role in *path Ox3* because the energetically lowest pathway only proceeds at the triplet PES and the three oxidation processes are associated with the reduction from highest oxidation state, V^V (VO_2^+), to V^{III} (VO^+) in all reaction channels.

A comparison between dehydrogenation and oxygenation processes shows that the allene is the most stable product (only 1.8 kcal/mol below propyne), 6.7 and 15.4 kcal/mol below acetone and propanaldehyde, respectively. Moreover, the allene and the propyne formation along the *paths Deh1* and *Deh2*, respectively, takes place, overcoming an energy barrier of 35.0 and 41.1 kcal/mol, respectively, from the product complexes (taking account of the existence of **CP-*Deh1*** and **CP-*Deh2***, respectively), while in *paths Ox1* and *Ox2*, the products are obtained from the product complexes climbing up barrier heights of 49.2 and 45.8 kcal/mol, respectively.

Finally, in Figure 5, the most favorable reaction pathways for the rearrangement of $VO_2^+ + C_3H_6$ along the dehydrogenation, *Deh1*, and oxygenation, *Ox1*, processes are depicted. Both reactive channels comprise a spin-state change, provided the spin inversion is sufficiently effective and the CPs, **CP-*Deh1*** and **CP-*Ox***, are appropriately positioned; the reaction pathway follows the sequence **s-VO$_2^+$ + s-C$_2$H$_6$ → s-1V → s-TS1-D1 → s-2-D1 → CP-*Deh1* → t-TS2-D1 → t-3-D1 → t-V(OH)$_2^+$ + s-Allene** for *Deh1*, while path *Ox1* takes place along **s-VO$_2^+$ + s-C$_2$H$_6$ → CP-*Ox* → t-1O → t-TS1-O1 → t-2-O1 → t-VO$^+$ + s-Acetone**.

Comparison with Other Related Reactions. We have performed a comparison of the present study (three dehydrogenation and three oxidation processes) with our previous works to provide valuable information about their reactivity patterns: (i) the reaction between **s-VO$_2^+$** and C_2H_4, where the most thermodynamic and kinetic products correspond to the oxidation process to yield preferentially **t-VO**$^+$ + CH_3CHO;[66] (ii) a dehydrogenation reaction **s-VO$_2^+$** + C_2H_6 to render **t-V(OH)$_2^+$** + C_2H_4.[67]

An analysis of the initial interaction complex of the reactants for the oxidation processes shows, in the case of the $VO_2^+ + C_2H_4$ reaction, a covalent interaction between V and one C atom of the ethene fragment, and this stable complex determines the following behavior of the system (associated with an O atom transfer between V and C atoms and 1,2-hydride transfers between both carbon atoms, or vice versa). However in *paths Ox1* and *Ox2* of the present work, the addition complex implies the formation of a three-membered ring between an O atom of the VO_2^+ moiety and the two carbon atoms of the ethylenic fragment of propene, followed by an intramolecular hydrogen transfer process between these carbon atoms, to render acetone or propanaldehyde. Considering the role of the switch from the s and t PESs, the crossing between them takes place in different regions along the most favorable reaction pathways. In the case of the reaction of VO_2^+ with C_2H_4 two CPs were characterized along two paths to render the same product, one of them before the product complex formation, and the other situated in the step connecting the reactant complex with the next corresponding to a C−O bond formation. Nevertheless, in *paths Ox1* and *Ox2*, the spin inversion, **CP-*Ox***, is directly located in the entrance channel during the formation of the reactant complex.

An analysis of the initial reactant complex for the dehydrogenation processes shows, in the reaction of VO_2^+ with C_2H_6, the formation of a three-member ring between the C−V−C frame, avoiding the formation of a V−C bond along the reaction

pathway, which is an intrinsic property of alkenes, such as the reactant complex of *paths Deh1* and *Deh2*, **s/t-1V**. While in the $VO_2^+ + C_2H_6$ reaction a β-elimination takes place from the ethane to the vanadyl frameworks, in *path Deh1* the first hydrogen transfer has a six-membered structure and the second one implies a migration where a pyramidal structure between the V atom and the three C atoms is formed; however, in *path Deh2* the first hydrogen transfer has a five-membered structure and the second one implies a four-membered structure. In the reaction of VO_2^+ with C_2H_6, the CP occurs in the path connecting the second C−H activation process with the most stable minima, at the exit channel. The same situation can be sensed in *path Deh2* (with **CP-*Deh2***), while in *path Deh1*, on the contrary, **CP-*Deh1*** opens the possibility of an energetically favorable channel at the triplet electronic state, just before the second hydrogen transfer process (the rate-limiting step) and being kinetically relevant.

In addition, we have compared our dehydrogenation and oxygenation processes with the reaction between VO_2^+ and propane to yield the propene elimination (*path a1-1*) and an ionic allyl complex (η^3-C_3H_5)V(O)-$(OH)^+$ along a dehydrogenation process (*path a2*), reported by Engeser et al.[37] The *path a1-1* to render propene and $V(OH)_2^+$ is similar to that of VO_2^+ and ethane (and *paths Deh1* and *Deh2*, previously analyzed) and also the CP situation (between the second transition structures and the global minima); these authors do not characterize the CP, and they point out that the switch between the spin states should control the outcome of the oxidation of propane by VO_2^+ along *path a1*. The *path a2* reported by Engeser et al. to render the allyl complex (η^3-C_3H_5)V(O)-$(OH)^+$ and the H_2 molecule can be compared to *path Deh3* and *path Ox3*, with similar steps associated with hydrogen transfer processes from a carbon atom to the vanadium atom and steps associated with hydrogen migrations from the oxygen atom of the vanadyl moiety to the hydrogen just joined at the vanadium atom.

Therefore, there is an increasing number of examples providing evidence that the chemical reactivity of VO_2^+ with saturated and unsaturated hydrocarbons is dominated by interactions of various surfaces (spin inversion), and this, in turn, means that such species show not only the reactivity characteristics for one electronic state, such as the ground state, but also the behavior of a second electronic state differing in spin.

4. Conclusions

The present calculations using density functional theory, B3LYP/6-311G(2d,p), provide thermochemical and kinetic information on the reaction between VO_2^+ ($^1A_1/^3A''$) and propene to yield different products along three dehydrogenation processes, $V(OH)_2^+$ ($^1\Sigma^+/^3\Sigma^-$) and allene (*path Deh1*), $V(OH)_2^+$ ($^1\Sigma^+/^3\Sigma^-$) and propyne (*path Deh2*), and VO_2^+ ($^1A_1/^3A''$), H_2, and allene (*path Deh3*), and along three oxidation processes to obtain VO^+ ($^1\Delta/^3\Sigma$) and acetone (*path Ox1*), VO^+ ($^1\Delta/^3\Sigma$) and propanaldehyde (*path Ox2*), and VO^+ ($^1\Delta/^3\Sigma$), H_2, and propenaldehyde (*path Ox3*). There are three crossing points between singlet and triplet electronic states, two along the dehydrogenation process (**CP-Deh1**, **CP-Deh2**) and one (**CP-*Ox***) that is common for the oxygenation process, p*ath-Ox1* and *path-Ox2*.

The theoretical data obtained may thus provide a helpful tool for the interpretation of the experimental findings and a useful guide for understanding the mechanism of other analogous reactions. From the comprehensive study on these reaction pathways the following conclusions can be drawn.

(i) The first step of the reaction between VO_2^+ ($^1A_1/^3A''$) and propene proceeds without any barrier to form reactive complexes along spontaneous processes. Only the reactive complexes **s/t-1V** and **s/t-1O** are the doors through which the dehydrogenation, *paths Deh*, and oxygenation, *paths Ox*, reaction pathways must pass to obtain the corresponding products.

(ii) The most kinetically and thermodynamically favorable reaction pathway takes place from **s-VO_2^+** + C_3H_6 reactants to **t-$V(OH_2)^+$** + allene products, in a dehydrogenation process. The first step corresponds with an addition process of **s-VO_2^+** to the C_1 atom along a barrierless energy profile to obtain an intermediate involving a cation $(VO_2^+)-(C_3H_6)$ interaction complex, **s-1V**. From this minimum, two consecutive C−H bond activation processes take place, associated with the hydrogen transfers (**s-TS1-D1** and **s-TS2-D1**) from the carbon to the oxygen atoms of the propene and vanadyl cation frameworks, respectively. Before the second C−H activation process, via **s-TS2-D1**, a crossing point, **CP-*Deh1***, has been characterized and the following steps occur preferentially at the triplet electronic state. Therefore, the presence of **CP-*Deh1*** should control the outcome of the reaction to the most stable combination of products, **t-$V(OH)_2^+$** and allene.

(iii) Although the allene formation along *path Deh1* is the most stable product, the propyne formation along *path Deh2* is only1.8 kcal/mol above the allene. A crossing point, **CP-*Deh2***, between s and t states has been localized just after the second hydrogen transfer process (not the rate-limiting step), so this CP is not kinetically relevant.

(iv) In the oxidation processes, the s−t spin inversion, **CP-*Ox***, takes place during the formation without barrier of the reactant complexes **s/t-1O** at the entrance channel. Therefore, from the **t-1O** minimum the reaction pathway will be energetically favorable along the t state, toward formation of the **t-2-O1** product complex, via an intramolecular hydrogen transfer **t-TS1-O1** to finally yield acetone and the **t-VO^+** cation, or toward formation of the **t-2-O2** product complex, via the **t-TS1-O2** to finally obtain propanaldehyde and the **t-VO^+** cation. However, to achieve the different oxidation products, it must overcome a considerable energy barrier from the respective product complexes.

(v) The present results can lead us to understand deeply the mechanism of the title reaction and can provide useful information for further experimental investigations and are expected to be helpful for understanding the chemical reactivity of VO_2^+ with saturated and unsaturated hydrocarbons.

Acknowledgment. This work is supported by DGI (project BQU2000-1425-C03-02 and BQU2003-04168-C03-03). L.G. acknowledges the Ministerio de Ciencia y Tecnología for providing a doctoral grant. J.R.S. thanks "Fundació Bancaixa-Universitat Jaume I" for financing a research stay at this University and Brazilian Funding Agencies FAPESP, CAPES, and FUNDUNESP. Computer facilities of the Servei d'Informàtica (Universitat Jaume I) are also acknowledged.

Supporting Information Available: Energies and geometries of all stationary points localized are summarized in S1−S72. This material is available free of charge via Internet at http://pubs.acs.org.

OM050971T